Case Studies and Field Applications of Cyclic Pressuremeter Test to Liquefaction Damaged Ground by Noto Peninsula Earthquake in 2024, Japan

Études de cas et application sur le terrain d'un essai de pressiomètre cyclique sur sol endommagé par liquéfaction lors du tremblement de terre de la péninsule de Noto en 2024, au Japon

Youngchuel Kwon[1#], *Akiyoshi* Kamura[2], *Keigo* Azuno[3], *Shotaro* Kubota[4], *Tomoko* Sasaki[4], *Shiro* Ohta[4], and *Motoki* Kazama[2,4]

[1]*Tohoku Institute of Technology, Dept. of Civil Engineering and Management, 35-1 Yagiyama, Taihaku, Sendai, Japan*
[2]*Tohoku University, Graduate School of Engineering, Dept. of Civil and Environmental Engineering, 6-6-06, Aramaki, Aza-Aoba, Aoba-ku, Sendai, Japan*
[3]*Chuo Kaihatsu Corporation, 3-4-2 Nishi-Aoki, Kawaguchi-shi, Saitama, Japan*
[4]*Kawasaki Geological Engineering, 2-11-15, Mita, Minato-ku, Tokyo, Japan*
[#]*Corresponding author: kwonyc17@tohtech.ac.jp*

ABSTRACT

In earthquake-prone countries such as Japan, the behaviour and seismic performance of foundation ground during large earthquakes determines the seismic stability of infrastructure structures. To date, pressuremeter tests have only been applied to monotonic loading and unloading. We are currently developing a cyclic pressuremeter test to better understand the dynamic properties of the ground. Since disturbance of soil samples and stress release affect the accurate estimation of soil dynamic properties, it is beneficial to estimate soil dynamic properties in situ without soil sampling to obtain more reliable results. Another major goal of this test method is to investigate the resistance performance of soil against liquefaction. The Noto Peninsula earthquake that occurred in Japan in January 2024 caused great damage in the Hokuriku region of Japan. Among the damages, the lateral flow damage due to liquefaction that occurred in Uchinada Town, Kahoku District, Ishikawa Prefecture was particularly noteworthy. Here, we report the results of a cyclic pressure meter test conducted on the damaged ground.

RESUME

Dans les pays exposés aux tremblements de terre comme le Japon, le comportement et la performance des fondations lors des grands séismes déterminent la stabilité sismique des infrastructures. Jusqu'à présent, les essais de pressiomètre n'ont été appliqués qu'au chargement et au déchargement monotones.Notre équipe développe actuellement une méthode innovante d'essai de pressiomètre cyclique pour saisir les propriétés dynamiques du sol. La perturbation des échantillons de sol et la libération de stress pouvant affecter l'estimation exacte des propriétés dynamiques du sol, il est avantageux d'estimer ces propriétés directement in situ, sans échantillonnage, afin d'obtenir des résultats plus fiables. Un objectif majeur de cette méthode d'essai est d'étudier la résistance du sol à la liquéfaction. Le tremblement de terre survenu en janvier 2024 dans la péninsule de Noto a causé d'importants dégâts dans la région de Hokuriku. Parmi les dommages, ceux causés par la liquéfaction dans la ville d'Uchinada, dans le district de Kahoku, préfecture d'Ishikawa, étaient particulièrement remarquables. Dans ce contexte, nous présentons les résultats d'un essai de pressiomètre cyclique effectué sur le sol endommagé. Ces résultats visent à fournir des informations cruciales pour mieux comprendre les mécanismes de la liquéfaction et améliorer les mesures de prévention dans les futures constructions sismiquement stables.

Keywords: cyclic pressuremeter test; liquefaction potential; stiffness degradation; sandy soils

1. Introduction

On January 1, 2024, a magnitude 7.5 earthquake struck the Noto Peninsula in Ishikawa Prefecture. The Modified Mercalli Intensity scale recorded levels of X to XI in both Shiga Town and Wajima City, as shown in Fig. 1. The earthquake resulted in over 1,500 casualties and caused damage to more than 8,500 buildings. Additionally, it led to significant destruction, including disruptions to electricity, water supplies, and the transportation network, due to crustal deformations, tsunamis, and lateral flows caused by liquefaction (Government of Japan, 2024).

The earthquake resulted in liquefaction and lateral flow damage across a broad region, extending from

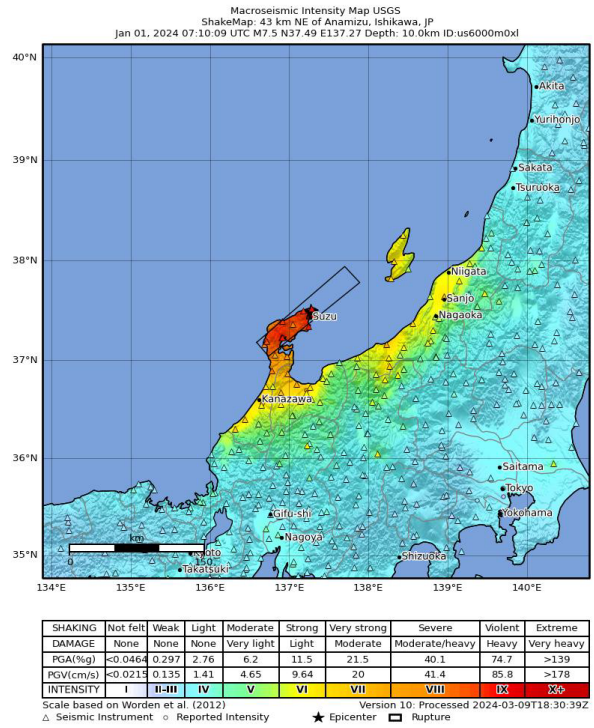

Figure 1. Seismic intensity recorded during the Noto Peninsula Earthquake in Japan (Source: USGS National Earthquake Information Center, PDE)

Figure 2. Damages from liquefaction in Uchinada Town

Fukui Prefecture to Niigata Prefecture in the north. A notable aspect of the liquefaction in the Noto area is that it occurred in many inland locations. The Noto Peninsula is characterized by its fine sand, which is easily deposited by seasonal winds coming from the sea. This leads to the formation of dunes, making the area particularly susceptible to liquefaction. Ultimately, it is believed that high groundwater levels near inland waterfronts contributed to the extensive liquefaction damage caused by the earthquake (Suppasria et al., 2024).

Japan is widely recognized for its susceptibility to earthquakes and has suffered considerable damage from liquefaction-induced lateral flow in coastal regions during strong seismic events. As a result, the seismic resistance and performance of the foundation ground are crucial for ensuring the safety of essential infrastructure during earthquakes. Researchers have made efforts to assess the seismic performance of these grounds at the in-situ level by developing various evaluation methods, one of which is the pressuremeter test.

Research on the pressuremeter as an in-situ testing method has mainly focused on monotonic geotechnical issues. However, several research groups have recently started adapting pressuremeter tests to evaluate the dynamic geotechnical properties of foundation soils (Kamura and Kazama 2021, Karagiannopoulos et al. 2021, Théo et al. 2024). The authors have developed a cyclic pressuremeter test system, along with a specified testing procedure. This system is designed to assess the dynamic properties under in-situ conditions by applying both loading and unloading forces to the ground. The development of this field test method aims to reduce the disturbance and stress reproducibility issues caused by sampling, which have been persistent challenges in geotechnical engineering.

This paper provides an overview of the cyclic pressuremeter testing system developed by our research group. Additionally, we will discuss some testing results as an application of this system at a site in Uchinada Town, Ishikawa Prefecture, Japan, where lateral flow occurred due to liquefaction following the Noto Peninsula Earthquake in 2024.

2. Cyclic pressuremeter test and testing procedure

Evaluation methods for geotechnical properties, based on continuum mechanics and expressed in a hollow cylindrical coordinate system, are widely utilized. The authors have been developing a system known as the cyclic pressuremeter test (CPMT), which enhances this method by allowing for cyclic loading in situ.

Fig. 3 illustrates the testing procedure for the CPMT proposed in this study, which closely resembles the traditional Menard pressuremeter test. The novel aspect introduced in this study is the cyclic loading process, in which cylindrical forces are applied to the soil through the injection and drainage of water into the probe. The cyclic loading process involves subjecting soils to repeated compression and release in order to measure stiffness degradation and their response to dynamic loading. Theoretically, soils respond to cyclic loading by losing strength and stiffness, generating excess pore water pressure, and experiencing cyclic softening, as depicted in Fig. 4. This process is repeated by incrementally increasing the starting pressure of the cyclic loading and measuring the stiffness degradation and changes in pore water pressure in the surrounding ground at each stage.

The pressuremeter tester features a probe that applies pressure to the cavity wall, a control and measurement unit for assessing wall pressure and displacement, a pressure generator, and tubes and cables connecting these components as depicted in Fig. 5. The pressure generator is a device that expands and contracts the membrane of the probe by moving a piston, which is controlled by a servomotor, in and out of a cylinder filled with water.

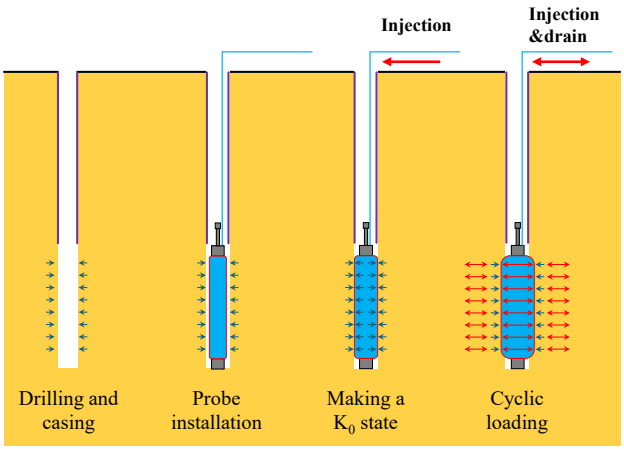

Figure 3. Testing procedure of the CPMT

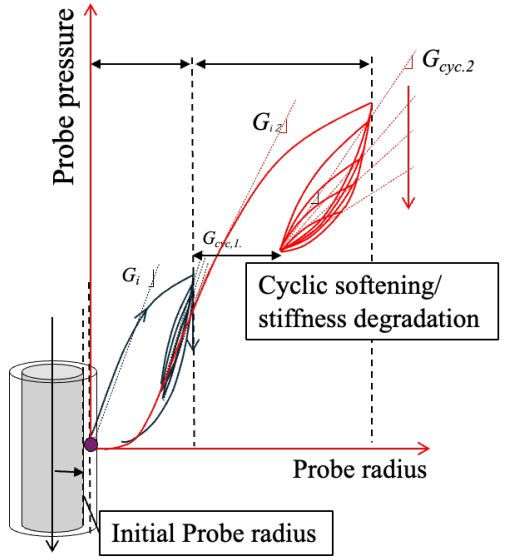

Figure 4. Cyclic loading scheme and stiffness degradation

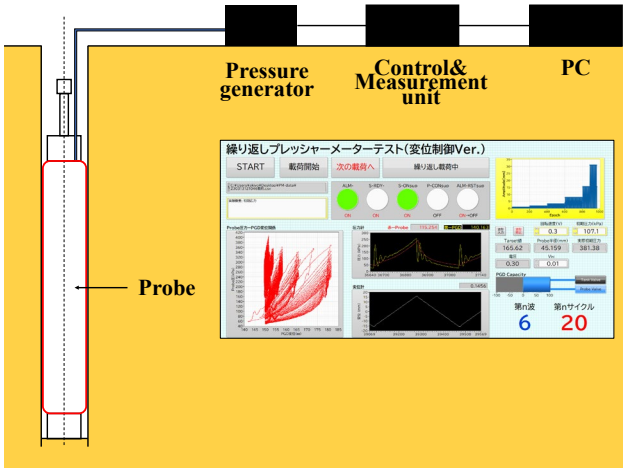

Figure 5. Hardware and software configuration of the CPMT for feedback control and data acquisition

This movement exerts pressure on the ground. The generator features a screw mechanism that converts the rotation of the servomotor into linear motion. The cDAQ manages the control and measurement of the entire system. During cyclic loading tests, it is essential to control the hardware, read measurements from various transducers, and perform feedback control at high speed to utilize the results for the next control cycle. To automate these tasks, software was developed using LabVIEW, a graphical programming language.

3. Field tests at Uchinada Town

3.1. Location and ground condition

The field experiment took place in August 2024 in Uchinada Town, which is located 13 kilometers north of Kanazawa Station in Japan. This area was developed through a reclamation project initiated by the Kanazawa Agricultural Land Office of the Ministry of Agriculture, Forestry, and Fisheries in 1963. The project involved cutting dunes and placing them in the Kahoku Lagoon. As a result, the area features extensive sandy soil that is deeply present throughout.

Uchinada Town is a typical area affected by the 2024 Noto Peninsula earthquake, where damage was primarily caused by liquefaction-induced lateral flow. Point Bh#01, shown in Fig. 6, is located near a north-south stream, suggesting that the groundwater level was likely high during the earthquake. As a result, the lateral flow damage at this location is classified as severe, in contrast to Bh#02, which is situated on the dune side and experienced less impact. The earthquake damage depicted in Fig. 2 was photographed at Point Bh#01. The CPMT for this study was also planned and conducted based on the findings from these two surveying points.

The soil conditions identified from the borehole investigation at two test points are summarized in Fig. 7. During the boring survey at location Bh#01, fine sand (Fs) was primarily found as embankment material used in land reclamation, extending up to 3.0 meters below the ground surface as depicted in Fig. 7(a). Beneath this layer, a thick original sandy dune bed was present, reaching down to a depth of 8.0 meters below ground level. Below the dune bed, there is a layer of silt (Ac). The groundwater level observed during the survey was approximately 5.0 meters below ground level. However, since this location is near a stream, it is expected that the groundwater level may fluctuate depending on the water levels of the stream at different times. The results from a separate portable dynamic cone penetration test (PDCPT) indicated that the groundwater level is at the same level as the ground surface. The N-value of the Fs layer is relatively low, i.e., less than 10, and the sd1 layer has a relatively high value of up to 30. The Ac layer was observed to have

an average N-value of about 10. In Bh#01, CPMT was conducted at four locations: three in the sandy layer at varying depths and one in the silt layer for comparison.

Bh#02 is situated approximately 100 meters northwest of Bh#01. Fig. 7(b) shows the boring logs obtained from the geotechnical survey conducted at this location. The stratigraphic analysis confirmed the presence of a loose sandy layer (sd1) extending down to G.L.-7.5m, followed by a dense sandy dune layer (sd2) that reaches G.L.-12.0m. The N-value for the sd1 layer is less than 10, indicating it was deposited in a loose state. In contrast, the sd2 layer has a significantly higher N-value of up to 50, indicating it is dense and compacted. At this site, CPMTs was performed at two points within the sd1 layer, where there is a potential for liquefaction.

Figure 6. Location of the test sites in Uchinada Town

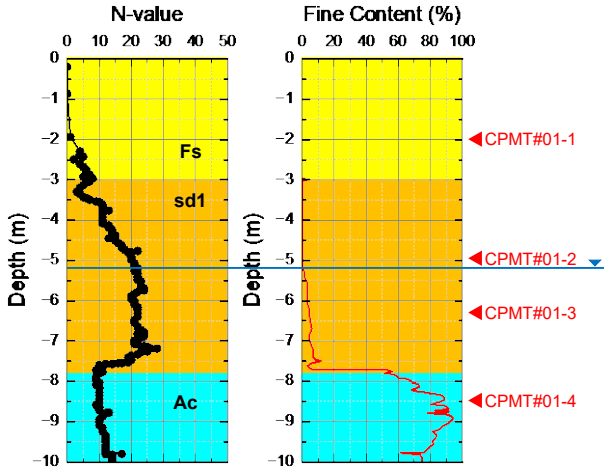

(a) Boring log of Bh#01

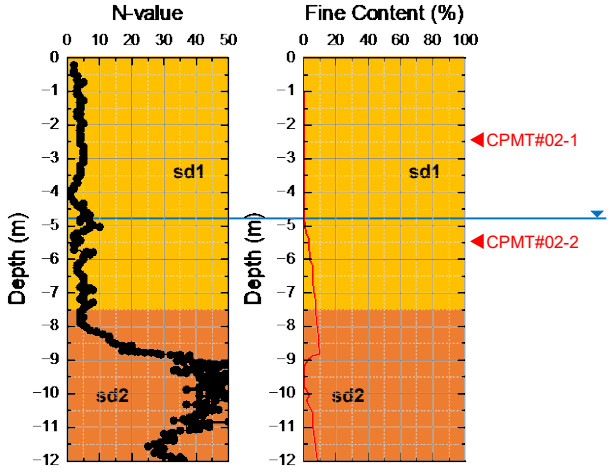

(b) Boring log of Bh#02

Figure 7. Ground condition at two test sites

3.2. Testing conditions

The test holes were drilled using the pre-boring method. To ensure accurate test results, it is important to minimize soil disturbance around the borehole. The diameter of the borehole was 90 mm, allowing for the full insertion of the probe, which is 80 mm in diameter before expansion, along with the necessary sensors.

Initial loading is essential to initiate the test under conditions similar to the original ground before drilling the test hole and to commence cyclic loading with the rubber membrane of the probe against the cavity wall. The initial loading pressure is calculated by determining the overburden pressure, which assumes the coefficient of earth pressure at rest, K_0 is equivalent to 0.5, and then adding the hydrostatic pressure to this overburden pressure. The ideal starting radius of the test cavity should be 45 mm. However, it is acknowledged that this radius may not be achievable at the beginning of the test due to various soil and field conditions, such as very loose sand or soft clay. Therefore, this study determined the starting point of the test based on changes in probe pressure, increasing the probe radius by 0.5 mm once it exceeds 40 mm.

During the cyclic loading phase, a constant amplitude was established for a predetermined number of loading cycles, which was then followed by the expansion of the cavity wall in the subsequent step. Fig. 8 provides a schematic diagram of the loading history used during the field test. This pattern entails setting the maximum radius or pressure from the previous step to the minimum value for loading in the next step. The radius or pressure being controlled remains consistent within each step. Fig. 8 illustrates only three steps to enhance reader understanding, but in total, 22 loading steps were performed, with each step involving 10 loading cycles.

To ensure accurate calibration, the tension of the rubber membrane on the probe must be subtracted from the measured probe pressure. In this study, the rubber membrane tension was assessed by generating the same loading history under constant external pressure condition in the water following cyclic loading in the ground.

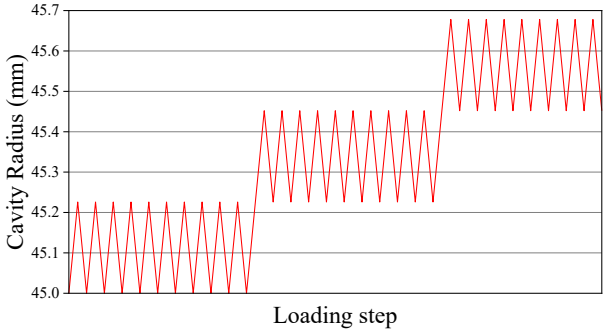

Figure 8. Loading history for the field tests (the maximum number of loading step is 22)

3.3. Field test results

3.3.1. Comparison of test results by soil type

The results of the experiments conducted on CPMT#01-4, which represents a silt layer (Ac), and CPMT#02-2, which represents a loose sand layer (sd1), are discussed here. As shown in Fig. 7, both sites have N-values of 1 and 3, indicating that they are very soft, with no significant differences between them. The silt layer is characterized by very low permeability and small particle sizes, suggesting that it is unlikely to be susceptible to earthquake-induced liquefaction. The soils were subjected to loading in up to 22 steps, with the waveforms illustrated in Fig. 8.

Fig. 9 illustrates the changes in probe pressure over time. In the silt soil, the probe pressure reached a maximum of 85 kPa from the 25 kPa, resulting in a difference of 60 kPa between these two values. In contrast, the difference in probe pressure in the sandy soil was 177 kPa, reflecting the changes in probe pressure due to subgrade reaction forces depending on soil type. Fig. 10 depicts the relationship between probe pressure and cavity radius. The tangent stiffness, derived from the relationship depicted in Fig. 10, is summarized in Fig. 11. Since the experiment was conducted under cyclic loading conditions while expanding the cavity wall, the change in stiffness at each loading step is a crucial evaluation factor.

The key points summarized from the figures indicate that the shear stiffness values of the silt subgrade exhibit only minor variations as the cyclic loading steps increase. Additionally, there is no significant degradation of shear stiffness observed within the same loading step. This trend remains consistent even under cyclic loading with an enlarged cavity wall. In the contrast, sandy soil demonstrates greater stiffness compared to silty soil, and its stiffness degradation is more significant under the cyclic loadings. In this test, the loading steps were designed to sequentially expand the cavity wall, resulting in an increase in stiffness as the number of loading steps increased. There were noticeable variations in stiffness within the same loading step when comparing sandy soil to silt soil. This suggests that the CMPT is effective in distinguishing the dynamic behaviors of these two different soil types: silt and sand.

Furthermore, Fig. 9 and Fig. 10 indicate that in loose sandy soils, the pressure ceases to increase once the probe pressure reaches approximately three times the overburden pressure. It is believed that the surrounding ground yields as the probe pressure increases, which is caused by the expansion of the cavity wall due to cyclic loading. This process concentrates some of the resulting strain in the uncased portion of the ground above the probe, ultimately leading to the collapse of the ground.

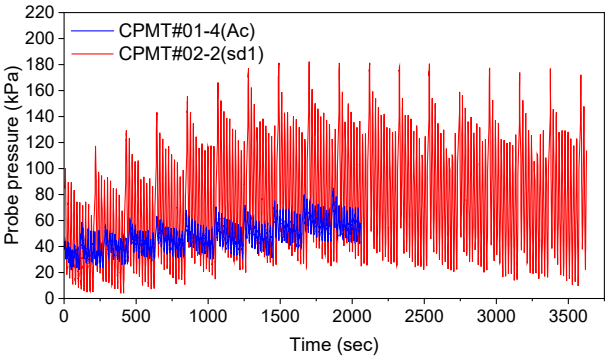

Figure 9. Variation of probe pressure with elapsed time in two difference soil types

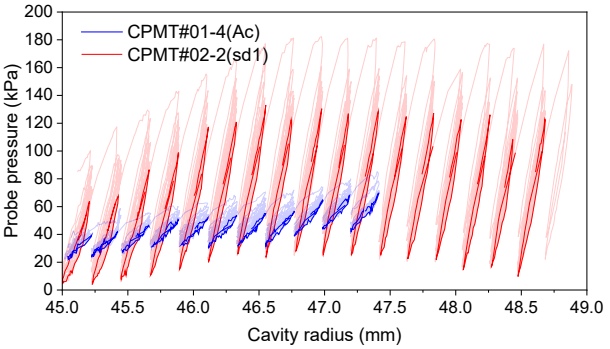

Figure 10. Probe pressure-cavity radius relation

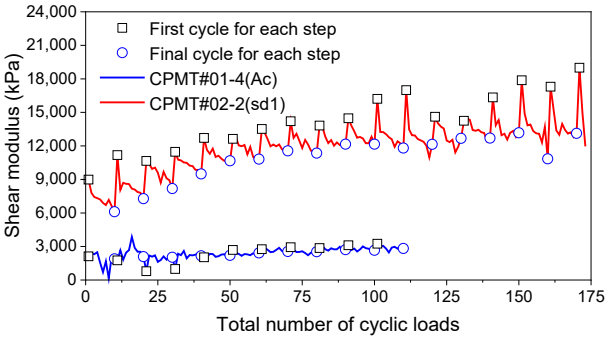

Figure 11. Shear modulus variation by the number of cyclic loadings

Although this is a technical extrapolation of the experiment, it is supported by the fact that the resistance was initially very high during the pull-out phase of the probe at the end of the experiment. It is concluded that when conducting CPMT in loose sandy ground, it is advised that the steel casing be installed directly above the probe to prevent the collapse of the cavity. Conversely, the results shown in Fig. 11 indicate that the change in shear stiffness is not significantly affected after the ground has yielded. It appears that the residual stiffness is largely retained, even following the yielding of the soils.

Furthermore, it is possible to cautiously estimate the strength of the soils based on the yield load obtained in the CPMT. This is supported by the observation that the pressure does not continue to increase beyond a certain ground reaction force, as

demonstrated in Fig. 9 and Fig. 10. The yield strength in looser soils was approximately twice the overburden pressure compared to CPMT#02-2. Consequently, further analytical studies are required to explore the relevance of relative density in estimating soil strength.

3.3.2. Test results for soils with different N-values

The test results will now be compared across different N-values within the same borehole to observe how soil behavior varies with these values. The following is a comparison of the test results for CPMT #01-1 to #01-3 in Fig. 7(a), where the N-values are 4, 13, and 20 respectively.

Due to the unpredictable level of soil disturbance in the borehole, the test began with an initial probe diameter of 45 mm. The probe pressure was then monitored up to 46 mm to determine whether the probe made contact with the surrounding ground. The diameter of the probe is designed to expand up to 50 mm as shown in Fig. 13. Fig.12 to Fig. 14 present the results of the CPMTs conducted in separately prepared holes without GS sampling. The probe pressure showed a significant increase when the probe radius exceeded 47 mm as shown in Fig. 12, for example. Subsequently, the pressure was measured to align with the N-value as expected (e.g., Fig. 14). Therefore, it is appropriate to establish the initial stress (or displacement) at approximately half of the effective overburden pressure, that means K_0=0.5, or with a probe radius of 46 mm as the starting point for the cyclic loadings.

Fig. 12 illustrates the pressure history of the probe after adjusting for the tension in the rubber membrane caused by the cyclic loading. The peak values recorded for each testing point were 74 kPa, 85 kPa, and 120 kPa, respectively. This data demonstrates that a higher N-value corresponds to an increased pressure needed to expand the probe. In essence, the findings effectively reflect the magnitude of the ground reaction force as a function of the N-value. Fig. 13 illustrates the relationship between cavity radius and probe pressure. The data presented in this figure is collected from the moment the probe contacts the cavity wall until the completion of the loading phase or the destruction of the soil structure, allowing for comparison. The comparison of these figures is challenging due to the varying timings of when the cavity wall is hit and when it is terminated. However, the results indicate that the probe pressure needed to increase the probe radius rises as the N-value increases.

Fig. 14 shows the results from Fig. 13, emphasizing the relationship between the number of cyclic loadings and the changes in shear stiffness. To ensure a precise comparison, CPMT #01-2 is shown in relation to the number of loadings that seem to have ed

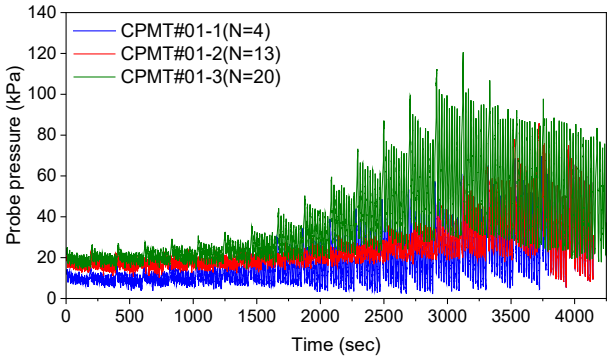

Figure 12. Variation in probe pressure as the N-value changes

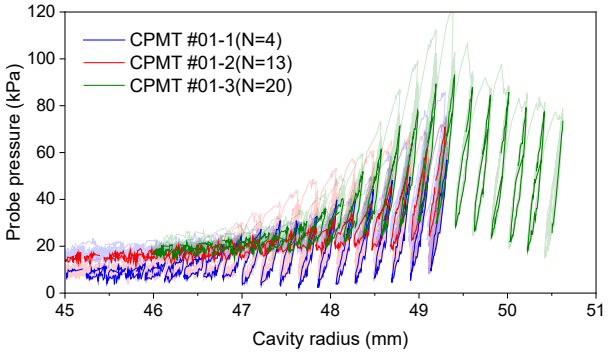

Figure 13. Relationship between probe pressure and cavity radius by N-value

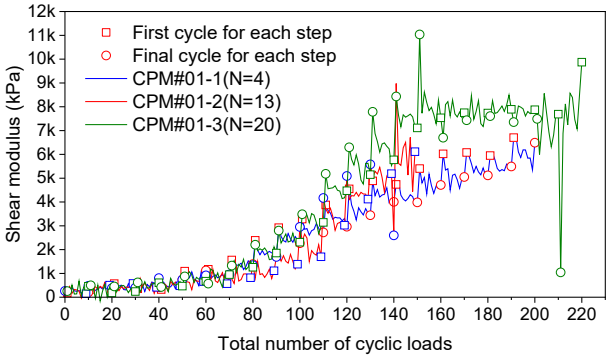

Figure 14. Variation of shear stiffness with the N-value

with the cavity wall. The figure indicates that the maximum values of shear stiffness were 6,500 kPa, 9,000 kPa, and 11,000 kPa, respectively. This demonstrates that the CPMT effectively captured the relationship between the N-value and shear stiffness, with higher N-values corresponding to greater shear stiffness. Additionally, the average decrease in stiffness per step increased with the N-value, measuring at 691 kPa, 813 kPa, and 1,105 kPa. This trend highlights significant stiffness degradation as a result of cyclic loading.

Fig. 12 and Fig. 13 present the maximum probe pressure limit, beyond which the value does not increase, particularly in relatively dense sand with relatively high N-values, such as CPMT#01-3. As

shown in Fig. 14, the shear stiffness remained constant after the pressure peak. It is suggested that the ground deformation caused by the expansion of the probe has a minimal influence. As the CPMTs involves extending the probe, it is assumed that the surrounding soils will become increasingly denser as the loading step increases. However, it is presumed that the effect of this densification is not a dominant factor. This phenomenon is likely caused because, within the area affected by the probe pressure, the soil becomes densified and displays elastic behavior. However, as the loading step increases, the extent of densification also expands, causing the soil outside the densified region to yield further. This ultimately leads to the failure of the generation of ground reaction forces after the peak of the probe pressure is reached.

Fig. 15 compares the stiffness degradation depicted in Fig. 14 across each test case for a specific cyclic loading step. As the point of contact with the cavity wall varies slightly in each test case, this figure is based on data from the load step when the earth pressure coefficient reaches zero. The differences among the various soil conditions were not distinctly noticeable; however, certain trends emerged concerning clay and sandy soils, as well as N-values. Notably, in CPMT#01-4, which featured a clayey soil, and CPMT#01-3, characterized by a comparatively high N-value, the stiffness degradation from the initial to the final cycle was approximately 0.9. On the other hand, it was about 0.75 for CPMT#01-1, which had the smallest N-value in the same cavity. This result is consistent with previous studies that the smaller the

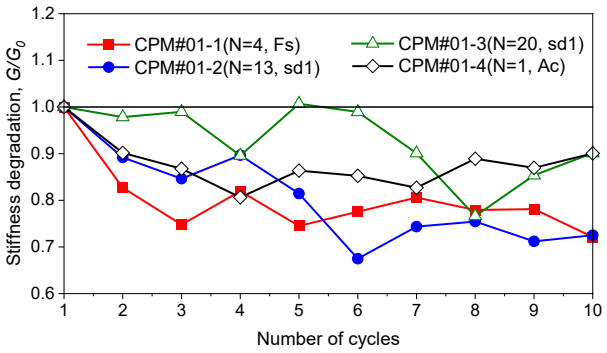

Figure 15. Stiffness degradation under various soil conditions occurs when K_0 is equivalent to 1.0

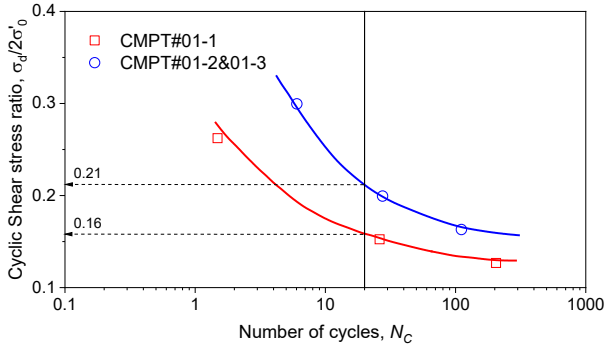

Figure 16. Comparison of liquefaction strength curves

particle size, the more stiffness degradation occurs when N-value is larger. It is challenging to observe significant stiffness degradation in these tests because the number of cyclic loadings per cycle was limited to 10, and the cavity wall was enlarged. However, the authors have confirmed stiffness degradation due to cyclic loadings in other experiments where they increased the number of loads per step without enlarging the cavity wall (Azuno et al. 2024, Kazama et al. 2024, Kwon et al. 2024).

The outcomes of an undrained triaxial compression test using undisturbed specimens taken from two different depths where CPMT was conducted are illustrated in Fig. 16. The figure shows the liquefaction strength curves, depicting the relationship between the number of cycles and the cyclic shear stress ratio, CSR. For CPMT#01-2 and CPMT#01-3, the liquefaction strength, RL_{20}, was measured at 0.21, with relatively high N values, which closely resembles the results observed in medium-density sandy soil. The CPMT#01-1 sample, which has a relatively small N value, exhibited an RL_{20} of 0.16. It was observed that the CPMT test results, based on the N-values presented in Fig. 12 through Fig. 14, are in good agreement with the triaxial test results obtained using undisturbed soil samples. Confirming the similarity between the trend of the CPMT results and the triaxial test results is a notable achievement; however, the compatibility of two values remains questionable. To enhance the utilization of the CPMT results, it is essential to evaluate its experimental results in relation to quantitative design constants like the CSR. This evaluation is still an area of ongoing research, and the authors believe it should be a focus for future studies.

4. Summary of findings

Authors present the results of a CPMT conducted in Uchinata Town, which experienced severe liquefaction flow damage due to the January 2024 Noto Peninsula earthquake. In the paper, the test results were analyzed based on variations in soil type and N-value.

The results from the study of silt and sandy soils revealed a significant difference in their ground reaction force and stiffness changes. Silt soil exhibited lower levels of ground reaction force and stiffness compared to sandy soil, with minimal changes in material properties observed under cyclic loading. In contrast, the stiffness of sandy soil decreased with each loading step, allowing for an estimation of the changes in its dynamic properties due to cyclic loading. The CPMT system used in this experiment effectively captured these changes.

Variations in results based on N-value were observed for some ground reaction forces and ground stiffness, although not as distinctly as anticipated. This

can be attributed to a loading pattern that expands the cavity wall and the relatively small number of loading cycles for each cyclic loading step. The results of this experiment indicate that in dense sandy conditions, the ground reaction force reaches its maximum at a pressure approximately three times the coefficient of lateral earth pressure at rest and subsequently decreases. Therefore, it can be anticipated that the experimental method used for expanding the cavity wall can effectively estimate both the strength and dynamic characteristics of the ground. We expect this to be confirmed in the future with monotonic pressuremeter experiments. One possible explanation for the lack of significant differences in the results related to the N-value is that the N-value of the local ground, which experienced liquefaction flow, may have differed from the observed N-value. This discrepancy is worth investigating further.

Two key findings were identified regarding the experimental methodology. Firstly, the level of disturbance to the cavity wall had a significant impact on the results, highlighting the need to pay greater attention to loose sandy soils. When CPMT was conducted in the same boring hole after soil sampling, there was no clear evidence that the probe made contact with the cavity, even after the maximum capacity of the testing equipment was reached. Damages to the cavity wall during the sampling process raises concern and has been shown to significantly affect results, particularly when sampling and CPMT are conducted sequentially in the same test hole. Additionally, when dealing with loose sandy ground, cyclic loading can lead to the collapse of the soil directly above the probe, which negatively impacts the test results. To achieve accurate results, it is crucial to extend the casing as far as possible to the location of the probe installation. In our second finding, we gain the experience to determine when the rubber membrane of the probe makes contact with the cavity wall, which varies depending on soil conditions. In fine-grained soils, the silt soil in this study, it is generally easy to identify when the initial pressure loading ends and when the subsequent cyclic loading starts. However, in sandy soils, particularly in loose soils, it can be challenging to determine the point at which the rubber membrane makes contact with the cavity wall. Additionally, assessing the subsequent cyclic loading based on the probe pressure rise is also difficult. In this field test, various test results indicated that the pressure should be set at half of the effective overburden.

Ultimately, the authors would like to provide some appendant comments regarding the experimental procedure. The field test involved conducting CPMT with various N-values by inserting a probe into the same borehole immediately after the GS samplings. However, the differences in the CMPT results among the various N-values were not apparent. The cause of this results was believed to be the significant disturbance around the borehole during the GS sampling. The GS sampler has a maximum outer diameter of 91 mm, and its outer tube rotates to cut off the surrounding soil. This structure contributes to the damage of the cavity wall, which increases the disturbance and affects the experimental results. The degree of disturbance in the cavity wall is difficult to assess, but it significantly impacts the test results especially in the loose sandy soils; therefore, it should be taken into account when analyzing them.

References

Azuno K., Ito R., Fukuhara M., Kwon Y., Kamura A., Kazama M. 2024. “Possibility of In Situ Cyclic Pressuremeter Test to Confirm Non-Liquefiable Ground”, 27th International conference on structural mechanics in Reactor Technology, Yokohama, Japan, 2024.

Cabinet office, Government of Japan, “Feature 1, 2024 Noto Peninsula earthquake”, Available at: [https://www.bousai.go.jp/kohou/kouhoubousai/r05/109/special_01.html], accessed: 23/01/2025.

Kamura A. and Kazama M. 2021. “Assessment of stiffness degradation of soil by in-situ cyclic loading using pressuremeter”, 6th International Conference on Geotechnical and Geophysical Site Characterization, Online conference, 26th-29th, September, 2021, https://doi.org/10.53243/ISC2020-153.

Karagiannopoulos P.G., Peronne M., Dang Q.H., Reiffsteck P., Benoît J. 2021. “Cyclic pressuremeter tests with pore pressure measurements, application to CSR evaluation”, 6th International Conference on Geotechnical and Geophysical Site Characterization, Online conference, 26th-29th, September, 2021, https://doi.org/10.53243/ISC2020-107.

Kazama, M., Kim, J., Kamura, A., Azuno, K. And Kwon, Y. 2024. “Challenges to Innovation of Liquefaction Prediction Technology”, Japanese Geotechnical Society Special Publication, Vol. 10, Issue. 4, pp. 64-78. https://doi.org/10.3208/jgssp.v10.KL-1-02

Kwon, Y., Kamura, A, Azuno, K., Kazama, M., Kawamata, Y., Ohya, Y., Mori, T., and Ito, R., 2024, “Development of cyclic pressuremeter test system for evaluate the dynamic propertiy of ground”, 18th World Conference Earthquake Engineering, 30th June-5th July, 2024, Milano, Italy.

Suppasria, A., Kitamura, M., Alexander, D., Setoc, S., and Imamura, F. 2024. “The 2024 Noto Peninsula earthquake: Preliminary observations and lessons to be learned” *International Journal of Disaster Risk Reduction*, Vol. 110, No. 104611,1-10, https://doi.org/10.1016/j.ijdrr.2024.10461

Théo, B., Catherine, J., Michel, R., Philippe, R., and Fabien, S. 2024, “Comparison between a New Rigid Dilatometer and the Ménard Pressuremeter in a Reconstituted Sand”, Geotechnical Testing Journal, Vol. 47, No. 4, pp. 879-894. https://doi.org/10.1520/GTJ20220292

USGS, “The 2024 Noto Peninsula earthquake: Preliminary observations and lessons to be learned.” Available at: https://earthquake.usgs.gov/earthquakes/eventpage/us6000m0xl/shakemap/intensity, accessed: 24/02/2025.